Feasibility of Friction Stir Welding for Joining and Microstructure Refinement in a ZK60 Magnesium Alloy

Sergey Mironov[1,4], Yoshinobu Motohashi[1], Tsutomu Ito[1], Alexandre Goloborodko[2], Kunio Funami[3] and Rastum Kaibyshev[4]

[1]*Research Center for Superplasticity, Faculty of Engineering, Ibaraki University, Hitachi 316-8511, Japan*
[2]*Department of Mechanical Engineering and Intelligent System, The University of Electro-Communications, Tokyo 182-8585, Japan*
[3]*Department of Machinery Engineering, Chiba Institute of Technology, Narashino 275-0016, Japan*
[4]*Institute for Metals Superplasticity Problems, Russian Academy of Sciences, 39 Khalturin Str., Ufa, 450001, Russia*

Feasibility of FSW to produce defect-free welds and for microstructure refinement in a ZK60 magnesium alloy has been examined over wide ranges of rotational and welding speeds. The results showed that joined-state was affected very much by the thickness of plates to be joined: for "thin" 3-mm thick plates, FSW was successful in a relatively wide range of welding conditions, whereas all "thick" 6-mm welds were found to be defective irrespective of rotational and welding speeds used. We have demonstrated that FSW is a very effective tool for microstructure refinement in the ZK60 alloy plates: A coarse, mm-scale, original grain structure was efficiently refined down to fine-grained range. It appears that second-phase particles containing Zr play an important role in the grain refinement.

Keywords: *friction stir welding, magnesium alloy, grain refinement*

1. Introduction

Magnesium alloy is one of the lightest metallic materials in practical use for structural applications. The promising balance of physical and mechanical properties of such alloys including high specific strength makes them very attractive for automotive and aerospace industries. However, despite the important benefits, magnesium alloys have been used for only limited applications due to their two principal drawbacks; generally poor weldability and low ductility.

Friction Stir Welding (FSW), a novel technology invented in 1991,[1)] appears to be a very promising processing technique for broadening the industrial application of magnesium alloys. As it is a solid-state process, FSW can avoid or limit solidification problems conventional fusion welding techniques have and thereby it can provide defect-free welds having good properties even in materials that are generally thought to be not appropriate for fusion welding. On the other hand, a material being subjected to FSW usually undergoes extreme levels of plastic deformation and thermal exposure, and these can lead to a significant microstructure refinement in the central part of the weld zone. This characteristic of the process allows us to consider FSW as a potential tool for superplastic property enhancement in magnesium alloys.

Considering the potential advantages of FSW, a number of research efforts have been made to evaluate effects of FSW on microstructures and various properties of magnesium alloys.[2–18)] Many studies on the ability of FSW to produce defect-free welds in some magnesium alloys have been published to date.[9,12–15)] However, as far as the authors know, the influence of FSW parameters on weldability of magnesium alloys has not yet been fully investigated and optimal "processing window" for joining has not been determined. On the other hand, the effect of FSW on microstructure refinement in magnesium alloys has been studied much extensively.[2–5,7–18)] Results of these studies have shown that FSW is generally suitable for grain refinement but the refining efficiency appears to be not very high and noticeable grain size reduction is typically observed only in cast alloys.[3,7–9)] In order to facilitate microstructure refinement, special approaches have been used in some works involving addition of ceramic particles into magnesium matrix[15–17)] or effective cooling of the material under FSW by liquid nitrogen.[18)]

It should be stressed that the above mentioned research attempts have focused mainly on Mg-Al based alloys. In contrast, less attention has been given to Mg-Zr based magnesium alloys. Zirconium is known to be an extremely potent grain refiner for magnesium alloys, and Mg-Zr based alloys have significant industrial importance due to their improved strength, ductility, creep resistance and so forth. More knowledge about feasibility of FSW for welding and microstructure refinement in these alloys is, therefore, required.

The work presented in this paper is part of a research project aimed to investigate the effects of FSW on microstructures and various properties of a ZK60 magnesium alloy belonging to Mg-Zn-Zr system. The present paper examines the feasibility of FSW to (i) produce defect-free welds and (ii) for microstructure refinement in the ZK60 and then evaluates the range of the appropriate processing conditions. For that purpose, a series of friction-stirred welds were made over wide ranges of rotational and traveling (welding) speeds for the plates having different thicknesses.

2. Experimental Procedure

The base material used in the present investigation was a commercial ZK60A magnesium alloy with nominal chemical composition (in mass%): Zn 4.8-6.2, Zr 0.45-0.8, other element $\leq$ 0.05, sum of other elements $\leq$0.30 and balance Mg. The material was received as a hot-extruded bar.

Table 1 FSW parameters used in the present study.

Designation of welds	Welding speed, V /mm×min^{-1}	Tool rotation speed, N/rotation per minute (rpm)	N/V
A1	100	600	6
A2	100	1000	10
A3	100	2000	20
A4	200	1200	6
A5	200	2000	10
A6	400	2000	5
B1	100	600	6
B2	100	800	8
B3	100	1000	10
B4	100	2000	20
B5	200	1200	6
B6	200	1400	7
B7	200	2000	10
B8	400	2000	5

Thickness of plate: A welds; 3 mm, B welds; 6 mm

Plates to be welded of about 50 mm in width were cut from the extruded bar perpendicular to the extrusion direction. Two sets of the plates of different thicknesses (t), 3 mm and 6 mm, were used in our study and the resulting welds are designated as "A" and "B", respectively. The plates were milled to provide a rectangular shape with parallel surfaces and then were butt-joined in pairs by a single FSW pass. To evaluate the ranges of appropriates processing conditions for the two thicknesses, FSW was performed at different combinations of rotational (600 to 2000 rpm) and travel (100 to 400 mm/min) speeds, as shown in Table 1. Welding tool has a shoulder having diameter of 14 mm and a M6 threaded cylindrical pin. The pin length was slightly shorter than the thickness of the plate (2.8 mm in the case of A-welds and 5.8 mm in B-ones). During FSW, the tool was tilted by 3° from the plate normal.

After the FSW, the obtained welds were cross-sectioned perpendicular to the welding direction, and were studied by optical microscopy (OM), scanning electron microscopy (SEM), electron back-scatter diffraction (EBSD) technique and by energy-dispersive X-ray (EDX) analysis. The welds were ground with water abrasive papers, mechanically polished with a final polishing step comprising of 0.1 μm alumina suspension, and chemically etched in the solution of 4.2 g picric acid + 65.8 ml ethanol + 10 ml acetic acid + 10 ml distilled water. A suitable surface finish for EBSD was obtained by applying a mechanical polishing in a similar fashion followed by electro-polishing in 6 : 3 : 1 = methanol : glycerine : nitric acid solution at approximately 5 to 10°C with an applied potential of 18 V.

Grain size was measured by the linear intercept method and volume fraction of second-phase particles was evaluated by the point-count technique. Chemical composition of the particles was examined with EDX.

High resolution EBSD analysis was conducted in a field emission gun SEM, equipped with TSL OIM™ EBSD system. Orientation mapping involving automatic beam scanning was performed and EBSD maps of 20000 to 50000 pixels with step (pixel) sizes of 0.1 to 0.5 μm, containing ~50 to 1000 grains, were obtained. In order to eliminate spurious boundaries caused by orientation noise, a lower limit boundary misorientation cut-off of 2° was used. All misorientation angles quoted are relative to the rotation axis with the minimum misorientation and 15° criterion was used to define low-angle versus high-angle boundaries. In the EBSD maps presented in this paper, low angle boundaries are depicted as white line, and high angle boundaries as black line.

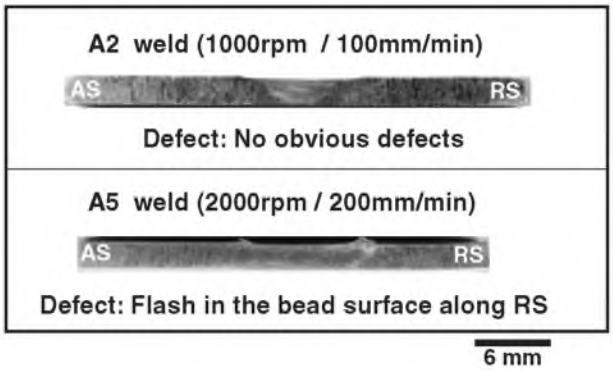

Fig. 1 Appearance of cross-sections of typical A-welds. AS: advancing side, RS: retreating side.

3. Results and Discussion

3.1 Weldability

In fusion welding, formed defects such as pores, solidification cracks, etc. deteriorate the weld quality and joint properties. Usually, friction stir welded (FSWed) joints are free from these defects. However, FSWed joints are prone to produce other defects like flash, tunnel-type defects, voids, groove-like defects, etc., most of which are caused by insufficient flow and/or consolidation of the material in friction stirred region. All the FSWed joints (hereafter referred to as "welds") fabricated in this investigation are analysed at first at a low-magnification to reveal the quality of friction stirred regions.

Typical optical macrographs of cross-sections of the welds are shown in Figs. 1 and 2. The relationship between welding parameters and quality of the welds are summarized in Fig. 3. Concerning A-welds, visual inspections for the welds showed that defect-free welds were obtained in almost all FSW conditions with the exception of A5 one (2000 rpm/200 mm/min, see Fig. 1). This means that FSW for 3-mm thick ZK60 magnesium alloy is feasible for joining in a relatively wide range of welding conditions. In A5 weld, flash was formed on the bead surface along RS. Formation of this defect during FSW is usually associated with excessive heat input and corresponding ejection of large mass of softened metal to the outside of the weld.[19]

Concerning B-welds, all of them are found to be defective irrespective of rotation and welding speeds used. At some combinations of low rotation (600–1000 rpm) and low welding (100 mm/min) speeds, inner tunnel-type defect was observed along weld centerline (see, *e.g.*, B1 and B3 welds in Fig. 2). The increment of the rotation speed to higher than 800 rpm significantly reduced the defect size,

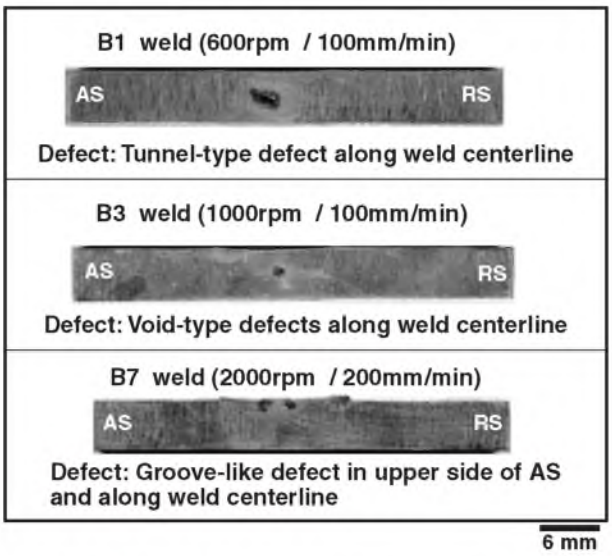

Fig. 2 Appearance of cross-sections of tipical B-welds.

transforming the tunnel-type defect into cluster of small voids. However, at rotation speeds higher than 1200 rpm, another groove-like defect was formed on the surface region of the weld (see *e.g.*, B7 weld in Fig. 2). At combinations of low welding (100 to 200 mm/min) and high rotation (1200 to 2000 rpm) speeds, the defect was located mostly along AS, whereas those at high welding (200 to 400 mm/min) and rotation (2000 rpm) speeds the defect was shifted toward weld centerline.

The tunnel-type defects as well as the groove-like ones are usually associated with insufficient material flow caused by insufficient heat input.[19–23] In the context of our study, of particular interest is the observation that weld quality of A- and B-welds is dramatically different at the same combinations of rotation and welding speeds (Fig. 3). This indicates that the thickness of the plate to be joined has strong effect on weld quality of ZK60. The defective nature of B-welds may be explained by the difference in temperature distribution during FSW. It has been reported that the maximum temperature to be reached in a FSW process is reciprocally proportional to specimen thickness.[24] Therefore, a main cause why the material flow in the thicker plates ($t = 6$ mm) was limited, which eventually led to the formation of defects, would be that the maximum temperature reached was lower than that in the thinner ones ($t = 3$ mm). It appears that the lower temperature reached in the thicker one made the material flow by crystallographic slips along non-basal planes less active and eventually forced the alloy to occur twinning (as will be described later) to compensate material flow. The twinning, however, would not be sufficient to compensate crystallographic slips, resulting in insufficient material flow.

3.2 Microstructure refinement

3.2.1 Initial microstructure

Characteristic microstructural features of as-received alloy (hereafter Base Metal (BM)) are summarized in Figs. 4 and 5. The Base Metal exhibits a partially recrystallized structure consisting of coarse fibrous-shaped grains, several hundred micrometers long and approximately 100 μm thick, lying parallel to the extrusion direction; they contain dense sub-structures and much finer equiaxed grains located mainly at the coarse grain boundaries regions (see Fig. 4(a)). The BM has a prominent fibre texture with $\langle 10\bar{1}0 \rangle$ direction (Fig. 4(b)) and misorientation-angle-distribution is shifted toward low-angles (Fig. 4(c)); fraction of high-angle boundaries consists of about 41% of total grain boundary area.

Second-phase particles in BM consist of a mixture of coarse (>1 μm) Mg-Zn base intermetallics precipitated mainly along grain and sub-grain boundaries (Fig. 5(a)), of coarse Zn-Zr base intermetallics which are preferentially sited within grains (Fig. 5(b)) and of fine dispersoids average diameter of which is smaller than <0.1 μm, homogeneously distributed in grain interiors (Fig. 5(c)). The total particles volume fraction measured by the point-count technique was approximately 11.1%. It is important to point out that some dispersoids seen in Fig. 5(c) have no distinct boundary with magnesium matrix and appear rather as white clouds. It is well known that a common characteristic feature of microstructures of magnesium alloys containing more than a few tenths percent soluble zirconium (including ZK60) is zirconium-rich cores that exist in most grains *e.g.*;[25] the cores are believed to be the products of a certain reaction during solidification.[26] The white clouds observed in Fig. 5(c) can be interpreted as the Zr-rich cores.

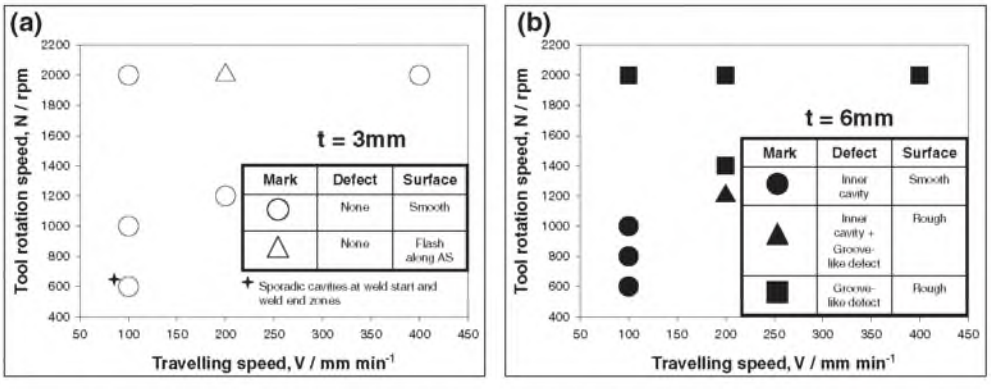

Fig. 3 Effect of FSW parameters on weld quality: (a) A-welds and (b) B-welds; t is the thickness of the weld.

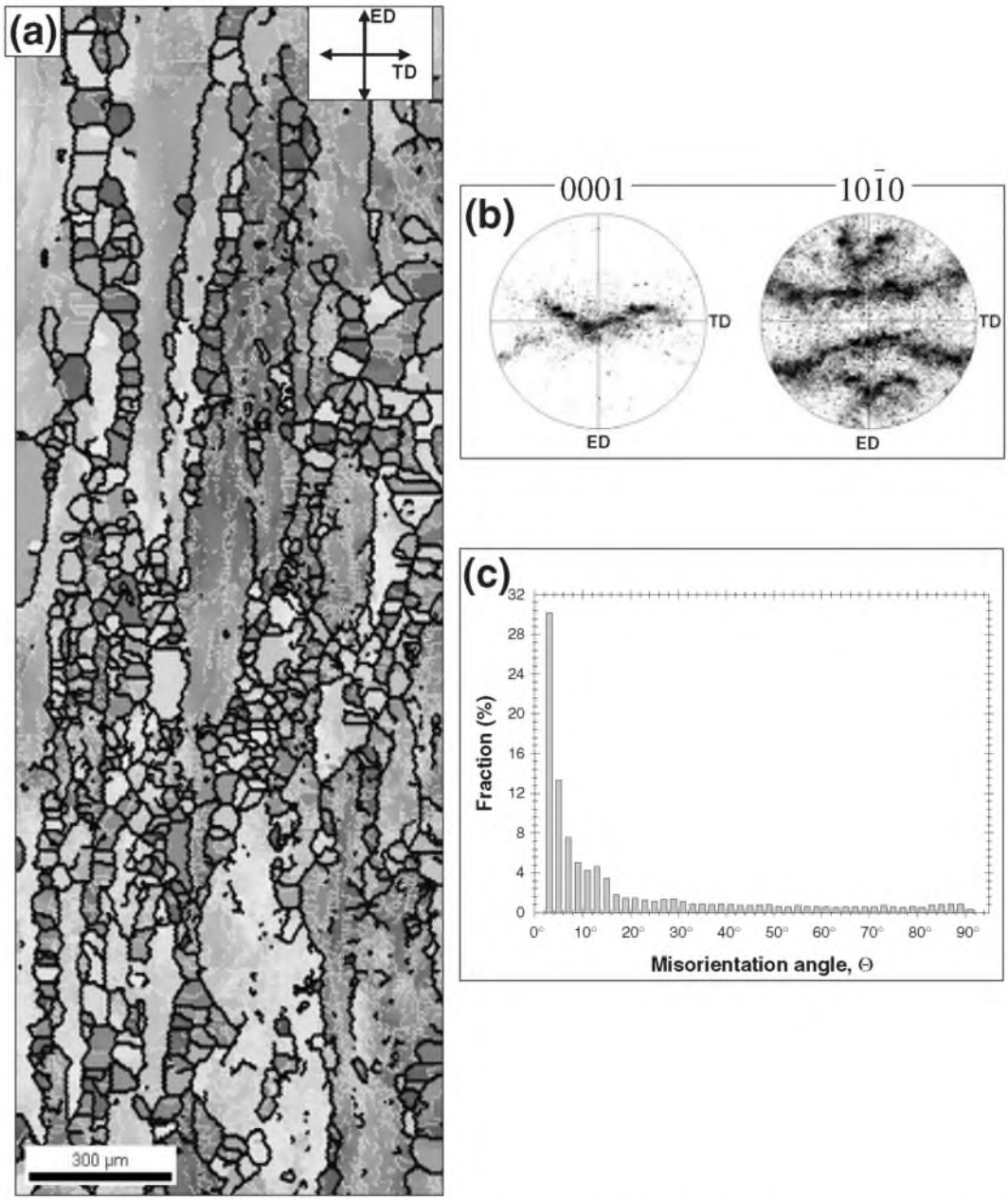

Fig. 4 Structure of BM: (a) EBSD-map (LABs and HABs are marked by thin white and bold black lines, respectively), (b) {0001} and {10$\bar{1}$0} pole figures, (c) misorientation angle distribution. ED and TD are extrusion and transversal directions, respectively.

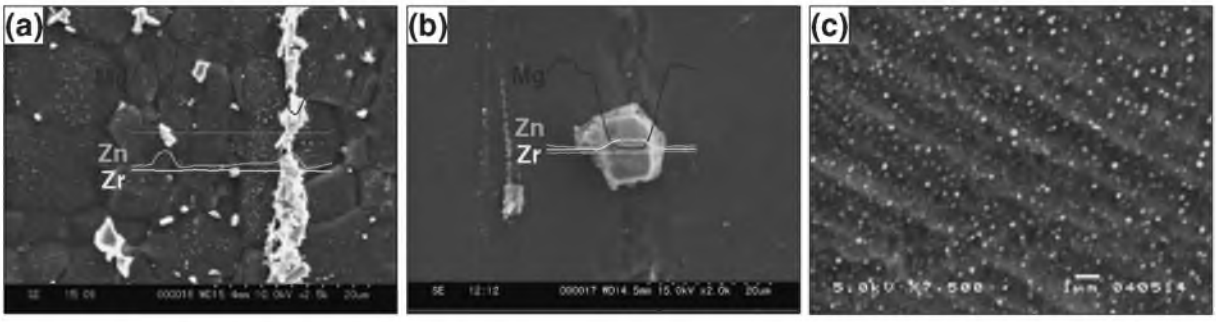

Fig. 5 Second-phase particles in Base Metal: (a) and (b) precipitation of coarse (>1 mm) particles along grain and subgrain boundaries and (c) homogeneous distribution of fine dispersoids (<0.1 mm) in grain interiors. Particles appear white. EDX profiles are shown in (a) and (b).

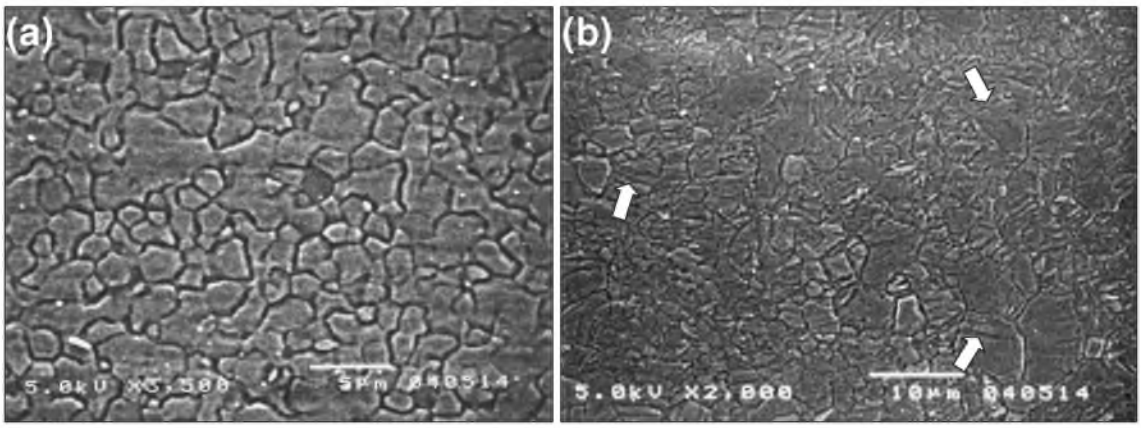

Fig. 6 Typical microstructures observed in (a) central part of weld nugget in A-welds and (b) B-welds. See text for details.

3.2.2 Morphology of structures and grain size in FSWed alloy

Typical examples of the microstructures found in the central part of the weld regions (hereafter "Stir Zone") of A- and B-welds are shown in Fig. 6(a) and (b), respectively. The microstructures are dominated by very fine grains. The A-welds exhibit a reasonably uniform grain structure consisting of equaxed recrystallized grains with little evidence of retained deformation. Grain structure of B-welds contains some lenticular-shaped features which can be interpreted as twins (arrowed).

In order to obtain a statistical view, more than 1000 grains were measured in each weld by linear intercept method and the resultant grain size statistics is summarized in Table 2. The measurements confirm the formation of fine-grained structures: the mean grain size ranges from 1.2 μm in B1 weld to 7.0 μm in A3 one. In this context it is important to point out that FSW is a very effective tool for microstructure refinement in ZK60.

In order to obtain more detailed information on the fine microstructures developed in Stir Zone, the central part of the weld nugget region of A1 and B6 welds were studied by using EBSD and the obtained results are shown in Figs. 7 and 8. The EBSD-maps in Figs. 7(a) and 8(a) demonstrate that the microstructures contain significant fraction of low-angle boundaries (LABs). These LABs comprised of about 30% and 35% of total grain boundary area in A1 and B6 welds, respectively. Additionally, some grains revealed in the EBSD-maps are not completely outlined by high angle boundaries. Such observations have been frequently associated with development of grain subdivision process *e.g.*[27] However, in our case, this issue may require additional detailed discussion.

Misorientation-angle distribution of A1 weld (Fig. 7(b)) is bimodal with a low angle peak and a wide peak in a misorientation range from 20 to 30 degrees. Misorientation distribution of B6 weld (Fig. 8(b)) additionally exhibits a weak peak in the vicinity of 90°. Misorientation distributions in magnesium alloys have not yet been investigated fully and the origin of these peaks is not completely clear. However, the weak peak near 90° may be associated with $\{10\bar{1}2\}$ twinning which produces 86° $\langle 1\bar{2}10\rangle$ misorientation in magnesium alloys *e.g.*[28]

Table 2 Summary of grain size statistics measured in weld nugget of different FSWed welds.

Designation of welds	Mean grain size, d/μm	Standard Deviation (μm)	Number of grain intercepts sampled
A-samples			
A1	2.0	1.1	1028
A2	3.9	2.2	1015
A3	7.0	3.8	1004
A4	4.9	2.9	1005
A5	5.9	3.5	1120
A6	4.0	2.3	1015
B-samples			
B1	1.2	0.6	1023
B2	2.9	1.7	1009
B3	1.3	0.9	1028
B4	3.6	2.1	1091
B5	2.7	2.2	1010
B6	2.1	1.8	1016
B7	2.0	1.6	1023
B8	2.4	1.6	1006

Orientation data were obtained from the EBSD maps and were arranged as $\{0001\}$ and $\{10\bar{1}0\}$ pole figures as shown in Figs. 7(c) and 8(c). It is seen that the grains are preferentially oriented such that $\langle 0001\rangle$ is near to WD. Formation of similar texture in the stirred zone of FSWed Mg-Al based alloys has been reported by many authors[2–5,8,13] and attributed to the alignment of $\{0001\}$ planes parallel to pin column surface during FSW.[29] As plastic strain of magnesium alloys at low temperatures arises mainly from slips on the close-packed basal $\{0001\}$ planes, such texture may significantly affect on the mechanical properties of FSWed Mg alloys.

To evaluate the effect of FSW conditions on microstructure refinement, the mean grains size was plotted against the tool rotation speed normalized by welding speed (N/V-value) in Fig. 9: The N/V-value is usually associated with heat input during FSW.[30] It is seen that the obtained grain size generally tends to increase with heat input but the trend is masked by large standard deviation of the measured grain size. Of particular interest is the observation that the thicker

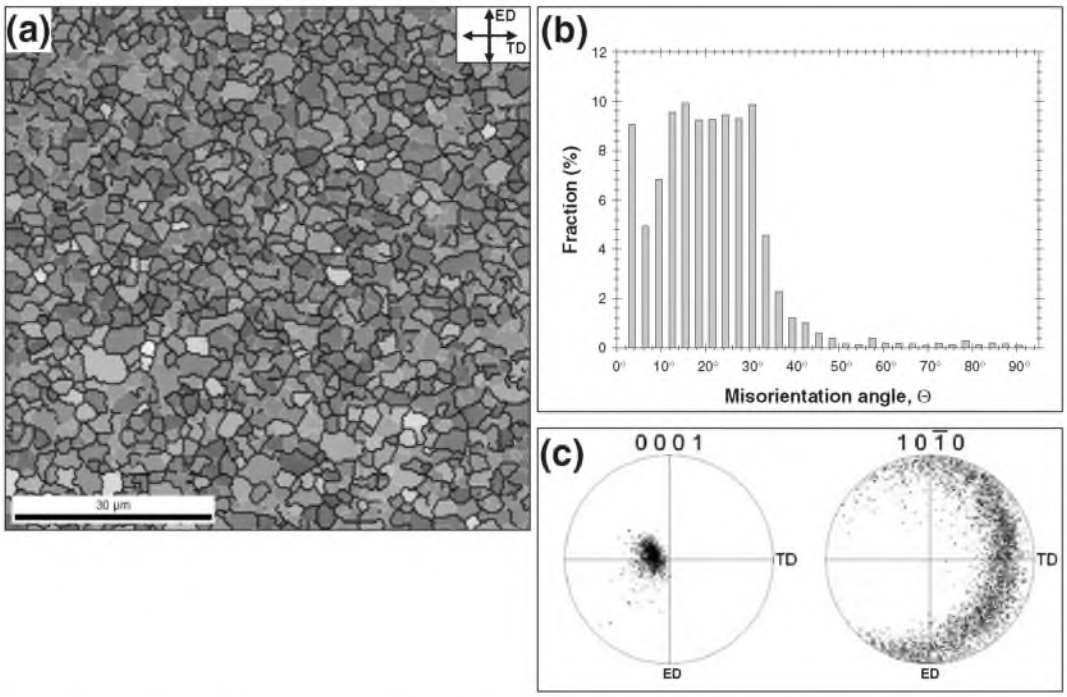

Fig. 7 EBSD characterization of stirred zone microstructure in A-weld: (a) EBSD-map, (b) misorientation angle distribution, (c) {0001} and {10$\bar{1}$0} pole figures.

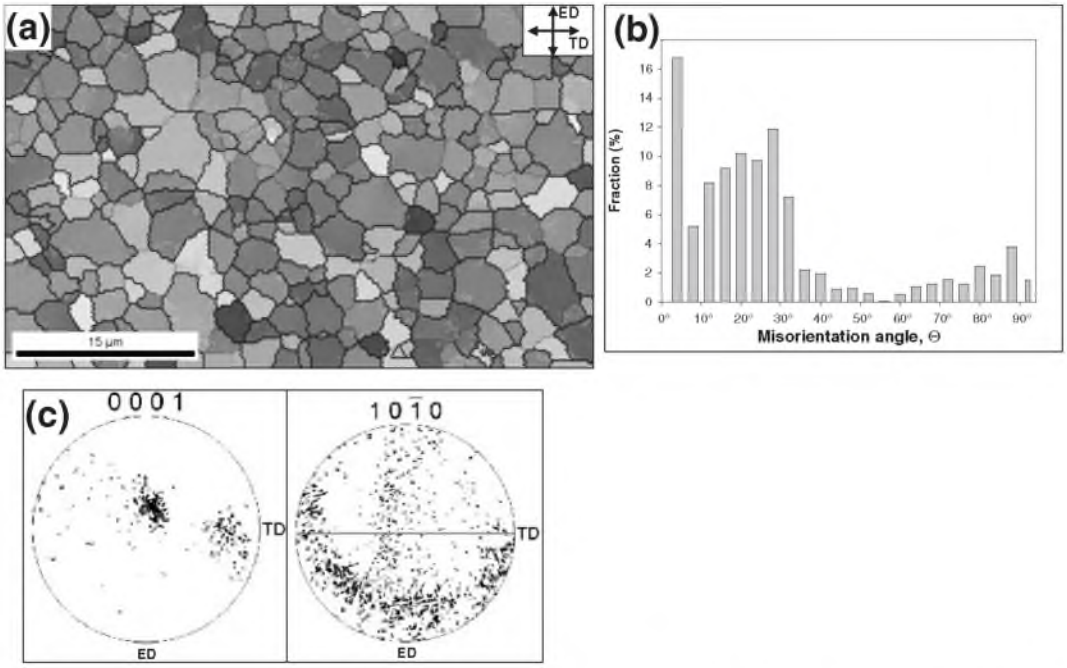

Fig. 8 EBSD characterization of stirred zone microstructure in B-weld: (a) EBSD-map, (b) misorientation angle distribution, (c) {0001} and {10$\bar{1}$0} pole figures.

B-welds generally exhibit smaller grain size than the thinner A-welds at the same N/V-value. Smaller mean grain size in B-samples together with higher LABs fraction and presence of twins support our assumption that B-welds were produced at lower heat input than the A-welds.

3.2.3 Effect of Zr on microstructure refinement

The present investigation has clearly demonstrated that the extremely coarse initial grain structure in ZK60 magnesium alloy can be dramatically refined into equaxed fine grain structures by means of FSW. Meanwhile it has been reported that FSW appears to be not so efficient for microstructure refinement in Mg-Al based alloys and noticeable grain size reduction in these materials has been only observed either in the case of cast alloys[3,7–9] or at the condition of incorporation of undeformable SiC, SiO_2 or C_{60} particles into the material.[15–17] The uniqueness of the ZK60 alloys is the existence of secondary particles containing Zr. It is well known that hard, micron-scale, second phase particles can

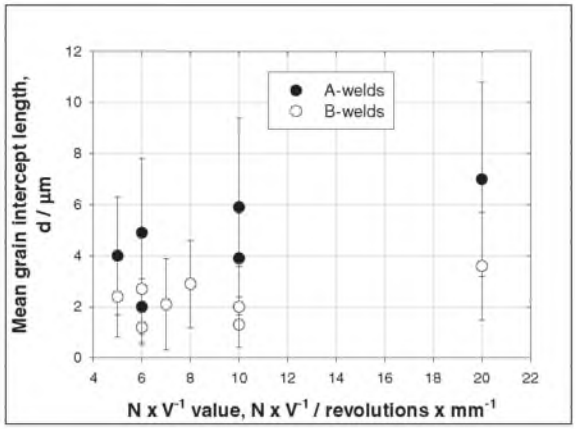

Fig. 9 Effect of FSW conditions on mean grain intercept length in SZ. The error bars correspond to standard deviation.

contribute grain refinement process.[31] In this regard, the superior grain refinement obtained in the ZK60 can be viewed from the particles containing Zr on the refining efficiency. Accordingly, precipitation behaviors and the correlation between the particles and microstructure evolution caused by FSW were considered in some detail for A1 weld for which the smallest grain size is obtained without any defect formation.

A typical precipitation pattern observed in Stir Zone is given in Fig. 10(a). Coarse (>1 μm in diameter) particles tend to align with a common direction. Similar particles alignment along flow patterns has already been reported in some magnesium[11,12] and aluminum alloys.[e.g.32] It seems that the reason for such particle distribution is still uncertain. However, it appears that kinematics of FSW process requires strain and strain rate variations that can cause particle segregation via material flow phenomena.

The particle volume fraction measured by the point-count method was 3.5%. This is significantly less than that of Base Metal (11.1 vol%) and, thereby, the particles appear to undergo partial or full dissolution during the FSW thermal cycle. A similar trend has been also observed in Mg-Al based alloys.[2,6,12] In order to identify the particles elemental composition in the Stir Zone, a total of 24 particles were studied by SEM-EDX technique. Due to limited spatial resolution, only coarse (>1 μm) particles were analyzed. All analyzed particles exhibit higher concentration of zinc and of zirconium than the surrounding material (a typical EDX line scan is shown in Fig. 10(b)) and they have been interpreted as kinds of Zn-Zr intermetallics. Meanwhile, almost no Mg-Zn intermetallics have been found within the present experiment.

Summing up the significant reduction of the particle volume fraction and the predominance of the Zn-Zr-rich precipitates observed in Stir Zone, it is supposed that many of constituent Mg-Zn intermetallics went into solution during the FSW process that caused a considerable temperature change as well as stirring of the material in the Stir Zone. On

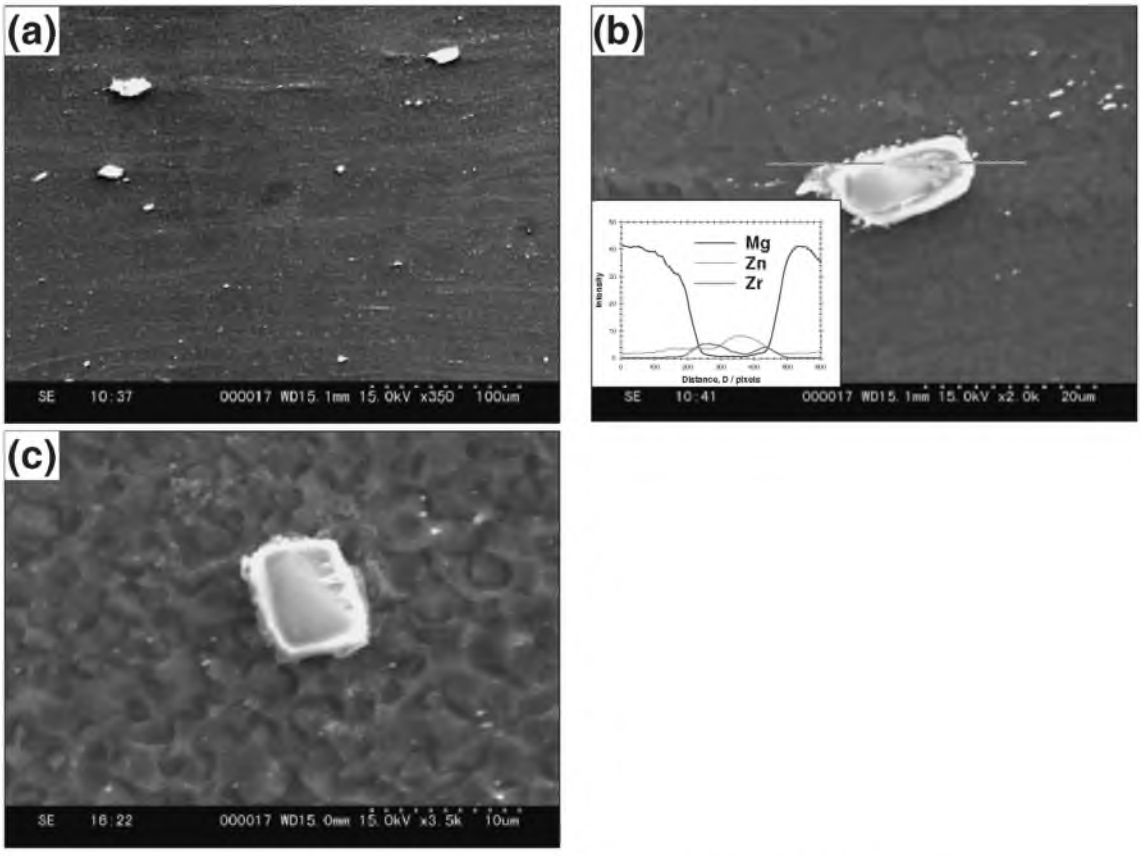

Fig. 10 Precipitation phenomena observed in Stir Zone: (a) alignment of coarse particles (>1 mm) along common direction, (b) typical EDX line scan across a coarse particle (elemental profiles for Mg, Zn and Zr are shown in the bottom left corner), (c) microstructure near a coarse particle. See text for details. Note: particles appear white.

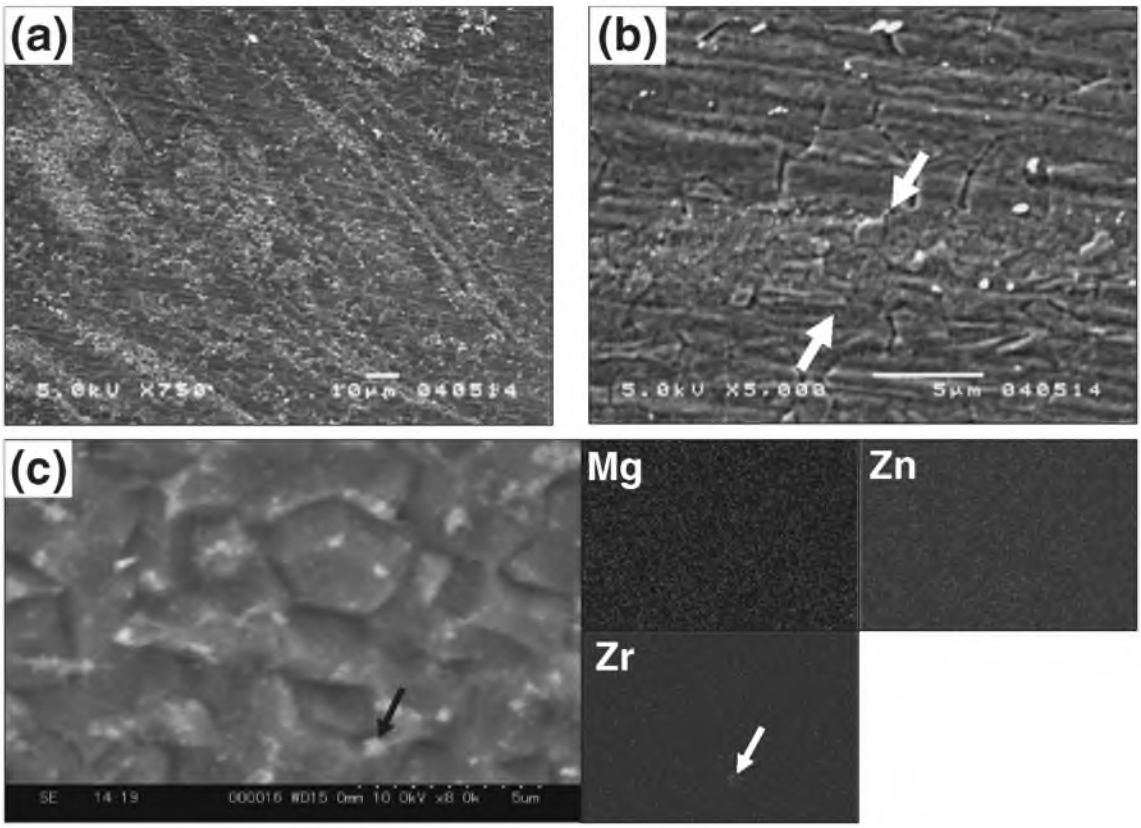

Fig. 11 Effect of Zr particles on microstructure refinement in ZK60: (a) white "clouds" of fine dispersoids, (b) fine-grained structure within a layer of fine dispersoids (arrowed), (c) EDX map of particle-rich region (a Zr-rich particle is arrowed)

the other hand, Zn-Zr intermetallics survived during the FSW and affected the microstructure evolution.

Low magnification observations of the microstructures have shown that there appeared white "clouds"-like regions on SEM images as shown in Fig. 11(a). A detailed inspection has indicated that the "clouds" consisted of sub-micron scale fine particles (Fig. 11(b)). It is also seen that average grain size within the "clouds" is significantly smaller than those in less particles regions, as seen in Fig. 11(b). The EDX mapping has shown that some of the particles (arrowed in Fig. 11(c)) are Zr-rich particles. It is generally believed that the Zr particles are effective grain refiners during solidification of magnesium alloys due to the low mismatch between magnesium and zirconium.[33] Our present study indicates that the particles containing Zr might have played an important role for the grain refinement during FSW of ZK60. Further studies will be necessary to discuss more in detail the role of particles containing Zr for the grain refinement caused by FSW process.

4. Conclusions

Feasibility of FSW process to produce defect-free weld and for microstructure refinement in a ZK60 magnesium alloy has been examined over wide ranges of rotational and welding speeds and the followings are the main conclusions obtained.

(1) Thickness of the alloy plate has the strongest effect on the weld quality of FSWed ZK60 alloy; Influences of the rotation and welding speeds are less significant in the present experimental range:

In the case of "thin" 3-mm thick plates, FSW is feasible in a relatively wide range of welding conditions, whereas all "thick" 6-mm welds have been found to be defective irrespective of rotational and welding speeds used. The defective nature of the thick welds seems to be attributed to insufficient heat input during FSW that would lead to less active crystallographic slips on non-basal planes.

(2) FSW is a very effective tool for microstructure refinement in ZK60. A single FSW pass refined mm-scale original grains down to fine-grained range irrespective of sample thickness and of rotational and welding speeds used. It appears that the superior grain refinement in ZK60 by means of FSW is associated with the particles containing Zr inherent to Mg-Zr alloys.

Acknowledgements

Authors would like to thank Dr. X. Yun and Mr. T. Sakuma for their help in realization of experiments. We also greatly acknowledge the Light Metal Educational Foundation for their financial support.

REFERENCES

1) W. M. Thomas: *Friction stir butt welding*, Int. Patent No. PCT/GB92/02203 (1991).
2) S. H. C. Park, Y. S. Sato and H. Kokawa: Scripta Mat. **49** (2003) 161–166.
3) C. I. Chang, C. J. Lee and J. C. Huang: Scripta Mat. **51** (2004) 509–514.
4) W. Woo, H. Choo, D. W. Brown, P. K. Liaw and Z. Feng: Scripta Mat.

54 (2006) 1859–1864.
5) Y. N. Wang, C. I. Chang, C. J. Lee, H. K. Lin and J. C. Huang: Scripta Mat. **55** (2006) 637–640.
6) A. H. Feng and Z. Y. Ma: Scripta Mat. **56** (2007) 397–400.
7) P. Cavaliere and P. P. De Marco: Mat. Sci. and Eng. **A462** (2007) 393–397.
8) C. J. Lee, J. C. Huang and X. H. Du: Scripta Mat. **56** (2007) 875–878.
9) P. Cavaliere and P. P. De Marco: Materials Characterization **58** (2007) 226–232.
10) P. Cavaliere and P. P. De Marco: J. Mat. Process. Tech. **184** (2007) 77–83.
11) D. Zhang, M. Suzuki and K. Maruyama: Scripta Mat. **52** (2005) 899–903.
12) W. Xunhong and W. Kuaishe: Mat. Sci. and Eng. **A431** (2006) 114–117.
13) F. Hung, C. Shinh, L. Chen and T. Lui: J. Alloys and Compounds **428** (2007) 106–114.
14) M. B. Kannan, W. Dietzel, R. Zeng, R. Zettler and J. F. dos Santos: Mat. Sci. and Eng. **A460–461** (2007) 243–250.
15) C. J. Lee, J. C. Huang and P. J. Hsieh: Scripta Mat. **54** (2006) 1415–1420.
16) Y. Morisada, H. Fujii, T. Nagaoka and M. Fukusumi: Mat. Sci. and Eng. **A433** (2006) 50–54.
17) Y. Morisada, H. Fujii, T. Nagaoka and M. Fukusumi: Scripta Mat. **55** (2006) 1067–1070.
18) C. I. Chang, X. H. Du and J. C. Huang: Scripta Mat. **57** (2007) 209–212.
19) Y. G. Kim, H. Fujii, T. Tsumura, T. Komazaki and K. Nakata: Mat. Sci. and Eng. **A415** (2006) 250–254.
20) Y. Zhao, S. Lin, L. Wu and F. Qu: Mat. Letters **59** (2005) 2948–2952.
21) H. Park, T. Kimura, T. Murakami, Y. Nagano, K. Nakata and M. Ushio: Mat. Sci. and Eng. **A371** (2004) 160–169.
22) Y. Chen, H. Liu and J. Feng: Mat. Sci. and Eng. **A420** (2006) 21–25.
23) H. Chen, K. Yan, T. Lin, S. Chen, C. Jiang and Y. Zhao: Mat. Sci. and Eng. **A433** (2006) 64–69.
24) T. Terasaki, T. Akiyama, T. Kitamura and M. Nakatani: Yousetsu Gakkai Ronbunnshu **23–1** (2005) 48–52.
25) M. Qian, D. H. StJohn and M. T. Frost: Scripta Mat. **46** (2002) 649–654.
26) E. F. Emley: *Principles of magnesium technology* (Pergamon Press, Oxford, 1966) p. 257–261.
27) P. B. Prangnell, J. R. Bowen and P. J. Apps: Mat. Sci. and Eng. **A357–377** (2004) 178–185.
28) M. D. Nave and M. R. Barnett: Scripta Mat. **51** (2004) 881–885.
29) S. H. C. Park, Y. S. Sato and H. Kokawa: Metall. Mater. Trans. **A34A** (2003) 987.
30) R. S. Mishra and Z. Y. Ma: Mat. Sci. and Eng. **R50** (2005) 1–78.
31) P. J. Apps, J. R. Bowen and P. B. Prangnell: Acta Mater. **51** (2003) 2811–2822.
32) M. A. Sutton, B. Yang, A. P. Reynolds and R. Taylor: Mat. Sci. and Eng. **A323** (2002) 160–166.
33) Y. Tamura, N. Kono, T. Motegi and E. Sato: J. Jpn. Inst. Light Metals **48** (1998) 185–189.